J Opt
https://doi.org/10.1007/s12596-021-00699-7

RESEARCH ARTICLE

Recent developments in polymer optical fiber strain sensors: A short review

Ayodele O. Soge[1] · Oluropo F. Dairo[1] · Modupe E. Sanyaolu[1] · Semiu O. Kareem[2]

Received: 21 September 2020 / Accepted: 12 February 2021

Abstract Polymer optical fiber (POF) strain sensors have attracted increasing attention owing to the unique features of polymer over silica such as lower Young's modulus, larger elastic strain limit, higher fracture toughness, biocompatibility, and lower production cost. Several POF strain sensors have been developed in recent years for applications in various technological fields, including structural health monitoring in civil construction and aerospace industries, biomedicine, and robotics. The principles of operation, prospects, and challenges of the POF strain sensors are discussed in this article under five broad categories: POF fiber Bragg grating sensors, intensity-based POF sensors, multimodal interference-based sensors, Brillouin-frequency-based sensors, and Fabry–Perot cavity sensor. This review aims to highlight areas where further research is required for improving the performance and operating range of POF strain sensors.

Keywords Polymer optical fiber · Polymer optical fiber strain sensors · Strain sensitivity · Viscoelasticity · Structural health monitoring

✉ Ayodele O. Soge
sogea@run.edu.ng; ayosoge@gmail.com

[1] Department of Physical Sciences, Faculty of Natural Sciences, Redeemer's University, PMB 230, Ede, Osun State, Nigeria

[2] Department of Physics, College of Basic Applied Science, Mountain Top University, Ibafo, Ogun State, Nigeria

Introduction

Polymer optical fiber (POF) sensors are emerging as an excellent alternative to their silica counterparts, especially when high flexibility and robustness are required [1]. Several sensing applications have practically explored some of the attractive features of POF over silica optical fiber (SOF) such as higher flexibility in bending, biocompatibility [2], higher failure strain [3], higher fracture toughness, and lower production cost. In addition to their immunity to electromagnetic interference, small size, and multiplexing capabilities – properties jointly shared with SOFs – POFs are also easily handled without special care due to their toughness and durability [4]. The higher diameter (about 1 mm) of POF, coupled with its flexibility, enables the application of low precision plastic connectors, which usually results in a lower-cost system [5, 6]. Besides, POFs also possess a higher numerical aperture that tolerates low-cost laser or light-emitting diode (LED) [7].

Furthermore, POF sensors offer enhanced sensitivity to strain, stress and force [8], pressure [9], and acoustic wave detection [10] due to the significantly lower Young's modulus of POF (2.2-3.8 GPa for polymethyl methacrylate and 2.0–2.4 GPa for polycarbonate) compared to SOF (68–74 GPa) [11, 12]. Additionally, POFs are suitable for measuring strain owing to their ductile behaviour and elastic strain limit compared to SOFs [6, 11]. For instance, polymethylmethacrylate (PMMA) has an elastic limit of around 10% compared to 1–3% for silica [11]. The strain sensitivity of an optical fiber sensor can be defined as the phase change in a lightwave propagating through the optical fiber per unit length of elongation [6, 11]. It is usually measured by subjecting the optical fiber to a pure axial strain [6, 11]. The strain sensitivity of a PMMA POF has been theoretically predicted to be 132.6×10^5 rads

Published online: 15 March 2021

m^{-1} using the Pockel's constants for bulk PMMA, which is 15% greater than that of bulk silica, 115×10^5 rads m^{-1} [6, 11]. The measurement of strain and stress is essential in several technological fields, including structural health monitoring in civil construction [13] and aerospace [14] industries, biomedicine, [15], and robotics [16]. Moreover, the large negative thermo-optic coefficient of polymer compared with the small positive thermo-optic coefficient of silica [17–19] endows POF sensors with improved sensitivity to temperature variations [20, 21]. The negative thermo-optic coefficient also presents new possibilities for temperature compensation in POF strain sensors [6, 11]. The biocompatibility of POF [2] offers additional applications in the biomedical sector, and the water absorption in some polymers such as PMMA can be used for humidity monitoring [22, 23].

Some of the drawbacks of POFs are their high losses and their viscoelastic nature [24]. The viscoelasticity of polymers implies that their mechanical properties can vary remarkably depending on the duration and frequency of the applied strain [25]. POFs have a nonlinear response when strained and relaxed [26, 27] due to their viscoelastic nature. Although polymer viscoelasticity has been widely studied for bulk materials, the viscoelastic characteristic of POFs is expected to possess somewhat unique properties due to the elongated shape and drawing conditions [28]. Besides, viscoelasticity can introduce hysteresis and creep effects when cyclic loading is applied to the fiber, which can influence the accuracy of the sensor reading. It has been demonstrated that these effects can be reduced by thermally annealing the fibers [29]. The performances of the POF-based sensors can also be altered by annealing [24]. For instance, enhanced strain [30] and humidity [31] sensitivity of POF Bragg grating (POFBG) sensors and longer temperature operational range [32] have been reported. Additionally, the outcome of the investigation by Prospori et al. [24] showed that annealing the polymer optical fiber tends to increase the strain, stress, and force sensitivity of the photo-scribed POFBG sensor.

Moreover, the development of optical fiber sensors introduced new possibilities to monitor the mechanical health of structures [33]. Remarkably, the excellent performance of fiber sensors for distributed measurement of strain outclassed the existing sensor techniques resulting in their huge potentials for specific structural health monitoring applications [33]. The fiber sensors offer the great advantage of measuring strain distributed over the entire length of the fiber, thereby replacing several standard electrical transducers. For instance, POF sensors have the unique ability to measure high strain distributed along the fiber up to 40% using the optical time-domain reflectometry (OTDR) technique [33]. Additionally, the geometrical versatility of the fiber sensors eases their integration into various structures [33]. Also, the large core diameter and numerical aperture of the commonly used PMMA POF enable easy connection and handling on the construction site without the need for expensive or sensitive equipment [33]. Apart from enhancing the safety of structures, the maintenance cost can be reduced considerably through early detection and repair of damaged structures [33]. Liehr et al. [33] reported distributed POF OTDR strain sensors integrated into technical textiles for structural health monitoring of civil engineering structures and geotechnical structures. The POF strain sensors were fabricated using both PMMA POF and perfluorinated graded-index POF (PFGI-POF). The PMMA POF allows measurement of high strain up to 40% with a modest spatial resolution of up to 100 m, while PFGI-POF offers strain detection with a high spatial resolution of 10 cm up to 500 m length. The sensor-integrated textiles improved the mechanical properties of the structure while acting as excellent sensor support facilitating installation and sensor protection on the construction site. Different modal tests conducted confirmed that reliable detection of soil displacement and crack openings in masonry structures is possible using textile integrated standard PMMA POF. Thus, the distributed POF OTDR strain sensors exhibit great potential for the monitoring of extended structures, where strong deformations are expected, and the use of silica fiber sensors is restricted [33].

In recent years, various POF strain sensors have been developed to enhance the sensitivity and dynamic range of the sensing system for a wide range of applications. These sensors are reviewed in this paper under five categories: fiber Bragg grating sensors, intensity-based POF sensors, multimodal interference-based sensors, Brillouin-frequency-based sensors, and Fabry–Perot cavity sensor. The principles of operation, prospects, and challenges of the POF strain sensors are discussed. This study aims to highlight areas where further research is required for improving the performance and operating range of POF strain sensors.

POF fiber Bragg grating strain sensors

Strain sensing is one of the most common purposes of fiber Bragg grating (FBG) sensors, and numerous reports have been provided mostly on the FBGs inscribed in standard silica single mode fibers (SMFs) [34]. For instance, a strain sensitivity of 6.3 nm/% has been reported at ~800 nm [34, 35]. However, silica SMFs are relatively fragile and cannot withstand strains larger than ~3%. One solution to this problem is to employ polymer optical fibers (POFs) [34, 36] which have incredibly high flexibility and can sometimes withstand strains of 50% or larger [34, 37].

Therefore, FBGs inscribed in POFs (POFBGs) have attracted considerable attention to enhance the strain dynamic range of the sensors [1, 34].

Fasano et al. [38] reported a high-temperature-resistant FBG strain sensor inscribed for the first time in a solid-core polycarbonate microstructured optical fiber (mPOF). Polycarbonate (PC) optical fibers consist of the core made of polycarbonate, with a polyolefin-based material as the cladding. This material has become a top candidate for optical fiber fabrication owing to its well-balanced optical and mechanical properties. It is transparent to visible light [39], making it a natural alternative to PMMA. In addition, PC usually yields and breaks at elevated values of strain [39] and is highly flexible in bending. Thus, it is a suitable material for POF strain sensor. Additionally, its glass transition temperature (Tg) of 145 °C is one of the highest among transparent plastics, thereby resulting in a broader available temperature range. These properties make PC fibers particularly attractive for those applications requiring high-temperature-resistant polymer sensors, provided the specific application does not involve long-term exposure to a high-humidity environment at high temperature. Early investigations have shown that humid heat may cause premature aging of PC POFs [40].

The solid-core PC mPOF was fabricated by using a drill-and-draw technique starting from casting of plastic granulates [41]. The diameter of the final fiber was about 150 μm, whereas the core diameter was 7 μm. The FBG inscription into the PC mPOF was performed with a 50 mW CW HeCd laser operating at 325 nm (IK5751I-G, Kimmon) using phase mask technique. The FBG was characterised in terms of sensitivity to strain and temperature by using a fiber coupler, a supercontinuum source, and an optical spectrum analyser. The fiber was gradually stretched up to 3% (loading phase, "forward"), and then, the strain was slowly decreased until the original dimension was recovered (unloading phase, "reverse"). Figure 1a displays the strain response of the PC mPOFBG at room temperature. The Bragg wavelength exhibited a linear response over the strain range 0–3%, with a sensitivity of 0.701 ± 0.003 pm/με calculated by linear regression. Thus, the sensitivity compares well with 0.71 pm/με reported for PMMA 3-ring mPOFBGs at 850 nm [42] and 827 nm [43], and similar to 0.64 pm/με measured for a TOPAS 2-ring mPOFBG at 870 nm [44]. Moreover, no hysteresis was displayed by the fiber in the unloading phase, since the forward and reverse curves perfectly overlapped, as illustrated in Fig. 1a. Similarly, the strain sensitivity in the reverse phase was calculated to be the same as the forward one (0.701 ± 0.003 pm/με).

Figure 1b illustrates the temperature response of the unstrained PC mPOFBG. The PC mPOFBG displayed a linear response between room temperature (23.6 °C) and 125 °C, showing a negative Bragg wavelength shift with increasing temperature. No malfunctioning was also observed even at the highest temperatures. The maximum temperature applied in the characterisation of the PC grating (125 °C) was more significant than the one previously demonstrated using a high-Tg TOPAS mPOFBG (110 °C) [45], and well above the maximum operating temperature of PMMA (92 °C) reported in [46, 50]. Temperature sensitivity of − 29.99 ± 0.17 pm/°C in the forward test and − 29.78 ± 0.09 pm/°C in the backward test was calculated for the FBG over the temperature range of 23.6–125 °C. No significant hysteresis was observed as the temperature was ramped down, as also confirmed by the almost unaltered sensitivities. The thermal stability of the fiber was due to the high Tg (145 °C) of the PC and the combined effect of the two distinct annealing phases performed at 120 °C and 130 °C on the fiber. Early investigations have confirmed that the annealing process significantly contributes to enhancing the thermal stability of polymeric FBGs and extending the linearity in their response to temperature [46, 47]. Thus, PC FBGs represent a step towards the development of a reliable high-temperature-resistant polymer-based FBG technology. Moreover, the excellent thermal stability of the PC POFBGs, coupled with their ability to withstand high temperatures up to 125 °C, has qualified them as potential candidates for applications in automation technology and automotive.

Although POF-based FBG sensors have several advantages over their silica fiber counterpart such as a lower Young's modulus and a higher breaking strain, the slow viscous response of POF FBGs could be a potential problem [28]. This problem was investigated by performing a long-term quasi-static measurement of the response of POF FBGs for strain levels up to 0.9% and strain times of up to 50 min [28]. The POF-based FBG comprised an in-house fabricated PMMA mPOFs using a POF draw tower. An FBG was inscribed into the fiber using the phase mask technique [48]. The relaxed FBG peak wavelength was at 618.7 nm after annealing the fiber for 48 h at 85 °C. A silica fiber was used to launch light into the POF and collect the reflected response of the FBG. The initial length of the fiber was 14 cm and was subjected to a maximum strain of 0.9% avoiding too high strains that might cause material deformation [49]. The fiber was strained with the help of a motorised stage, and the fiber relaxation (recovery) was monitored through the reflected FBG peak. While the motorised stage moved consistently, due to the viscoelastic nature of polymer, the FBG peak had a time lag in relaxing to the initial position. The experiment was performed in a controlled environment with a temperature change of less than 2 °C, and the change of relative humidity (RH) was less than 2% to prevent cross-sensitivity. Yang et al. [49] demonstrated that the fiber, when

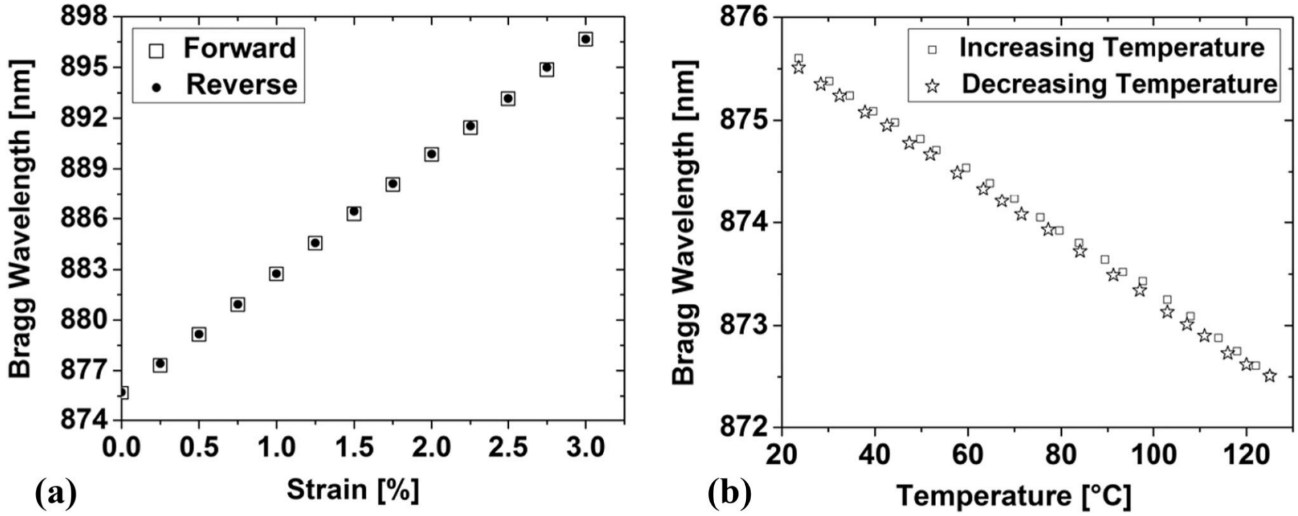

Fig. 1 **a** Strain response of the PC mPOFBG at room temperature. **b** Temperature response of the unstrained PC mPOFBG [38]

relaxing from strains of up to 0.9%, exhibited a two-phase recovery: initially fast linear (elastic driven) and subsequently slow nonlinear (viscoelastic driven) contraction. The linear elastic relaxation wavelength range depends both on the strain level and on the strain duration. The slow viscous wavelength regime of the POF-based FBG sensor was monitored for 10 repeated cycles of strain and relaxation. The experimental result showed that any hysteresis initially present was eliminated after enough strain relaxation cycles. Hence, the slow viscous response saturates while the fast elastic response, during which the sensor can rapidly follow the strain, stayed above 65% of the total wavelength interval. The authors claimed that if a POF FBG sensor is sufficiently pre-strained, then it can always follow the applied strains investigated in real time.

Cross-sensitivity to temperature and humidity is a major challenge for using POFBG to measure strain by monitoring wavelength shift because temperature and humidity variation can also cause wavelength shift [50]. To overcome this drawback, Min et al. [50] proposed a chirped mPOFBG based on taper technology for strain sensing application. The mPOFBG combined the merits of tapered chirped Bragg grating and fundamental POF characteristics. Previous investigations have shown that tapered Chirped FBGs (CFBGs) are effective for strain sensing with a 3-dB bandwidth modulation remaining insensitive to humidity and temperature variations [30]. Endlessly single-mode BDK-doped PMMA mPOF [51] was produced by using the centre hole doping technique. A CFBG was inscribed using the phase mask method (total length 10 mm) and a single 15 ns pulse from a 2.5 mJ pulsed Coherent Bragg Star Industrial-LN krypton fluoride (KrF) excimer laser at 248 nm. Figure 2 depicts the experimental set-up used for the strain characterisation of the CFBG. The

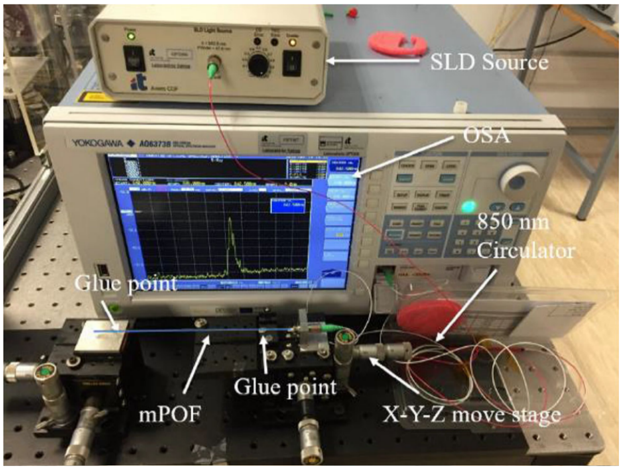

Fig. 2 Strain measurement set-up [50]

fiber was fixed with epoxy to avoid sliding. The axial strain was applied to the fiber through longitudinal displacement controlled by a 3D translation stage. The grating reflected spectrum was monitored using a super luminescent diode (Superlum SLD-371-HP1) and an optical spectrum analyser (Yokogawa AQ6373B) with 20 pm spectral resolution. Figure 3a shows how the reflected power spectrum of the grating changes with strain. As illustrated in Fig. 3a, a 12.62-cm section of POF had strain applied on the grating in 200 μm steps, causing a positive wavelength shift. Figure 3b indicates that the central wavelength of the grating increases with strain. The strain sensitivity of 0.90 ± 0.02 pm/με was obtained, higher than that of a uniform POFBG in the same material and geometry ($\sim$0.71 pm/με) due to the tapered etching of the fiber [52]. Figure 3c displays the bandwidth of the grating increase with strain, which could also be used to measure the strain

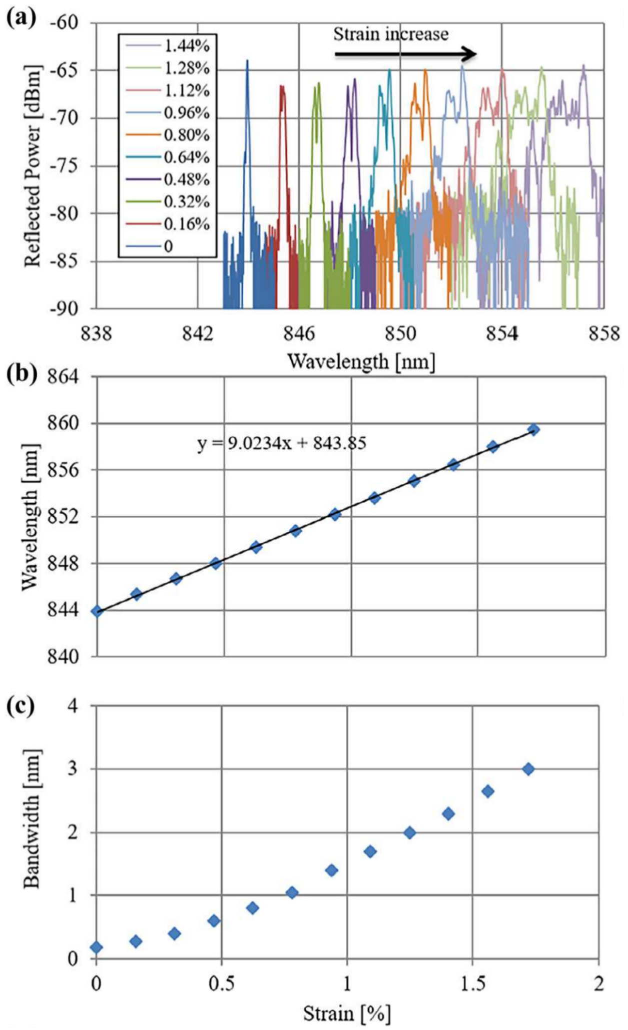

Fig. 3 **a** Spectral reflected power vs strain; **b** wavelength shift versus strain; **c** bandwidth versus strain [50]

sensitivity provided temperature and humidity sensitivities are compensated.

The experimental results obtained showed that the 3-dB bandwidth remained constant at 2.00 ± 0.05 nm over the temperature increase from 22 to 52 °C with 60% humidity and 1.25% strain. This result confirmed the temperature independent of the CFBG strain sensor. Besides, the 3-dB bandwidth decreases with increase in humidity and a sensitivity ∼ − 4.2 ± 0.4 pm/% was obtained under high strain condition and 60% humidity fluctuation. Thus, the excellent performance of the CFBG in POF is comparable to that of its silica counterpart. The grating response time was significantly improved by measuring the 3-dB bandwidth, which is a great benefit towards commercial strain sensing applications using POFBGs, especially under variable temperature and humidity conditions.

Intensity-based POF strain sensors

Leal-Junior et al. [53] reported a POF strain gauge based on the principle of light coupling between two fibers applied on a lower limb orthosis to measure the human–robot interaction forces. The advantages of this sensor include low cost, ease of implementation, and simplicity on signal processing since it is an intensity variation-based sensor [54]. Additionally, the proposed strain gauge does not suffer from cross-sensitivity to temperature. The fiber can be positioned on the structure without using glues or resins since the employed POF has 1 mm of diameter. Besides, the POF viscoelastic response does not produce errors on the sensor strain measurement because there is no stress directly applied to the fiber [7]. The light coupling principle employed on the POF strain gauge (POF-SG) is based on the misalignment between two POFs – illuminated POF and non-illuminated fiber POF. The misalignment between the two POFs causes power attenuation which is proportional to the strain on the structure that the fibers are attached.

The proposed POF sensor was applied to an active orthosis for knee rehabilitation exercises through flexion/extension cycles. The controller of the orthosis provided 10 different levels of robotic assistance on the flexion/extension movement. The POF strain gauge was tested at each one of these levels. The experimental results obtained displayed a good correlation between the optical and electronic strain gauges with root mean squared deviation (RMSD) of 1.87 Nm when all cycles were analysed, which represents a deviation of less than 8%. For the application, the proposed sensor presented higher stability than the electronic one, which can provide advantages on the rehabilitation exercises and on the inner controller of the device. However, the POF-SG does not possess the multiplexing capabilities of FBGs, which is desirable for measuring more points of interaction between the user and the robot. Therefore, the application of FBGs on the multipoint measurement of human robot interaction forces constitutes an area of further research to this application of the POF-SG.

Furthermore, Becker et al. [55] proposed a POF strain sensor based on the phase measurement of an intensity-modulated light wave using a step-index POF (SI-POF). The sensor scheme is simple and competitive. An LED can be used as the light source and an optical receiver is required to convert the intensity-modulated optical power at the end of the fiber into a modulated electrical voltage. When the fiber is strained, the modulation phase at the end of the fiber changes, resulting in a phase shift $\Delta\phi$.

The strain state of the sensing fiber can be observed using a commercially available low-cost integrated circuit to monitor the phase difference between the measured signal and a reference signal. The authors investigated the impact of strain on a SI-POF and evaluated the consequences for the responsivity of a strain sensor based on the phase measurement of an intensity-modulated signal. In comparison with a single-mode polymer optical fiber (SM-POF), the light propagation in a SI-POF (a multi-mode fiber) is affected by additional effects, including modal dispersion and the angular dependency of the refractive index of the strained fiber. Therefore, the geometrical deformation of the fiber and the impact on the angular-dependent refractive index were considered. By integrating the known effects into a novel fiber model, the authors were able to simulate the responsivity of the sensor for different scenarios and compared the predictions to experimentally obtained data.

In an ideal fiber, in which only one axial mode propagates, the phase of an intensity-modulated light wave is linear to the length L of the fiber:

$$\phi_{ideal}(L) = 2\pi \frac{L n_0 f_{mod}}{c_0} \quad (1)$$

where n_0 is the refractive index of the core, c_0 is the speed of light in vacuum, and f_{mod} is the modulation frequency. Considering only the length change due to strain and neglecting the impact on the refractive index, the ideal phase change can be expressed as:

$$\phi_{ideal} = \phi_{ideal}(L + \Delta L) - \phi_{ideal}(L) = 2\pi \frac{\Delta L n_0 f_{mod}}{c_0} = 2\pi \frac{\varepsilon L_0 n_0 f_{mod}}{c_0} \quad (2)$$

where ε is the strain which is defined as the ratio of the length change of the strained fiber ΔL to the length of the unstrained fiber L_0. Equation (2) shows the linear dependency of the ideal phase change on the strain. However, in the case of a real fiber, the development of the modulation phase in an SI-POF is not strictly linear to the length of the fiber due to influences such as modal and chromatic dispersion, attenuation, and scattering, this is also applicable to an unstrained SI-POF. Therefore, the modulation phase in an SI-POF, including the mentioned influences, is expressed as

$$\phi_{real}(L) = \phi_{ideal}(L) + \Delta\phi(L) \quad (3)$$

$\Delta\phi(L)$ accounts for the deviation of the development of the real modulation phase from the ideal phase, depending on the length of the fiber. Thus, Eq. (3) depicts the non-linear dependency of the modulation phase on the length of the fiber.

The responsivity of the sensor can be expressed as the ratio of the real phase change $\Delta\phi_{real}$ to the ideal phase change $\Delta\phi_{ideal}$:

$$R = \frac{\Delta\phi_{real}}{\Delta\phi_{ideal}} \quad (4)$$

$\Delta\phi_{real}$ is the modulation phase change which is obtained from two measurements at different strain states or from the simulations performed with the fiber model. The non-linear dependency of the modulation phase on the length of the fiber is considered by the fiber model.

Furthermore, the simulations with the fiber model led to the conclusion that the angular dependency of the refractive index was negligible. It was reported that the measured responsivities were larger than the simulated ones. This was possibly attributed to the Poisson's ratio of an SI-POF being larger than the assumed value of $n = 0.345$. It might also be caused by the assumed photoelastic constants since they were obtained for bulk PMMA, they could be different for an SI-POF as well. The results obtained also confirmed that the scattering behaviour of a SI-POF is strain-dependent, which was further proven by measuring the far field at the end of a SI-POF under different strain conditions. Additionally, the proposed sensor has excellent potentials for structural health monitoring and other applications considering the general benefits of fiber optical sensors (such as light weight, immune to electromagnetic interference) and particularly the advantages of POF. This is especially true since it has been shown that a SI-POF can be strained to more than 40% while maintaining its light-guiding properties [56].

Kamimura and Furukawa [57] demonstrated strain sensing based on a radiative emission–absorption mechanism using a dye-doped POF. The core and cladding of the fiber were doped with Coumarin 540A (donor) and Rhodamine 6G (acceptor), respectively. Compared to the conventional fiber-optic sensors based on FBG and Brillouin scattering, the strain sensor employed a simple and low-cost mechanism to detect stress by comparison of two luminescence peaks from a pair of energy transfer organic dyes. Figure 4a illustrates the principle of the POF strain sensor showing the donor/acceptor (D/A) dye pairs for the radiative emission–absorption mechanism doped in the optical fiber core and cladding, respectively.

The donor-exciting wavelength λ_{exD} is coupled to the core and propagates down the fiber. The donor dye in the core emits at the wavelength λ_{emD}. At locations where stress is applied to the fiber, the deformation induces λ_{emD} leaks to the cladding. It has been reported that doping luminescent dye in the optical fiber core enhances light leakage from the core to cladding [58]. Hence, after absorbing this leaking light, the acceptor dye in the cladding emits λ_{emA}, which is detected at the fiber output end and represents the extent of the stress load. The stress information can be displayed as a large phase shift by the strain POF sensor. The excitation and emission spectra of

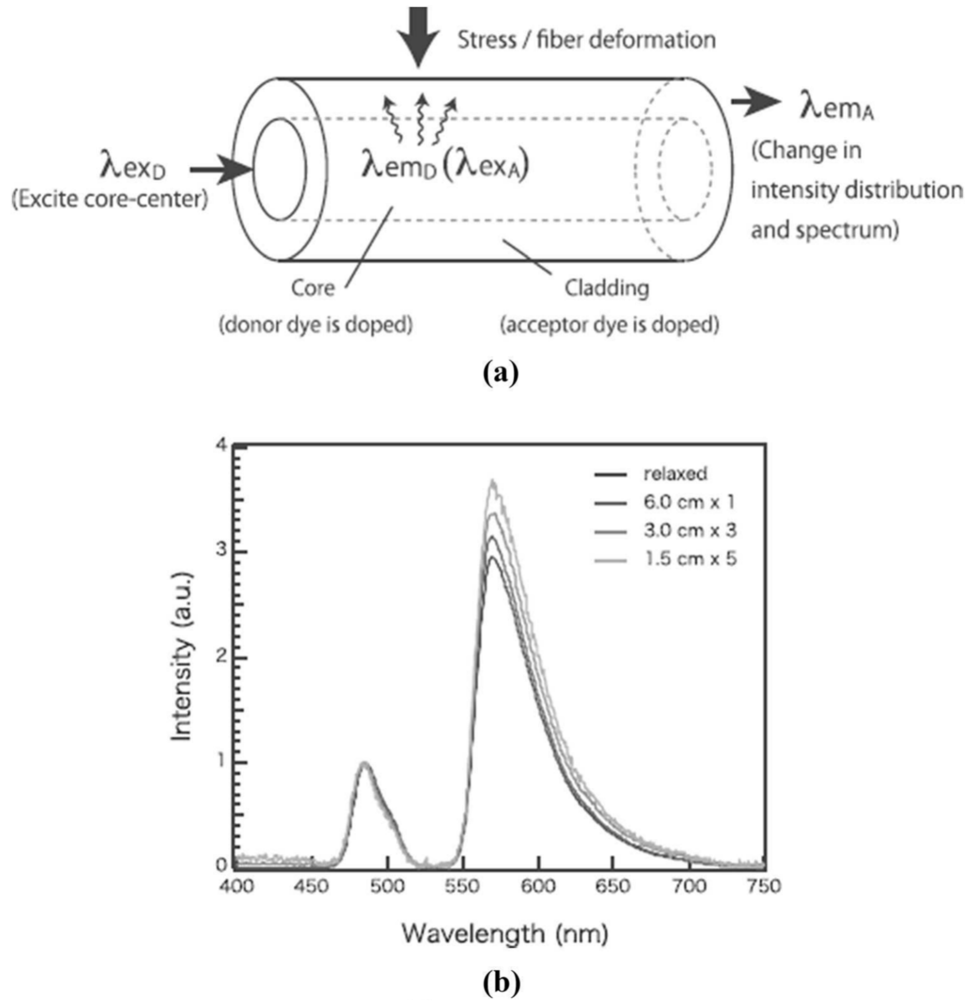

Fig. 4 **a** Principle of the POF strain sensor using the radiative emission absorption mechanism, **b** Output spectra of the fiber for different bending conditions. The fiber was either relaxed (straightened) or bent in loops with specific diameters [57]

the D/A dye pairs showed that λ_{emD} and λ_{emA} peaks are about 100 nm apart. This difference can be detected with simple optical components instead of the spectral analysis required in conventional fiber-optic sensors. Therefore, because of its simple structure and mechanism, it could be easily analysed in various types of situations at low installation and/or operational costs.

Measurements were taken for different λ_{exD} and λ_{exA} values, or either, to demonstrate the sensor principles. Stress was applied to the POF using macro-bending of the fiber [57]. The applied stress could be detected as an increase in cladding intensity. Due to this deformation, emission from the core dye leaks to the cladding and excites the cladding dye. For various laser wavelengths, the change in the near-field pattern and visible emission spectrum upon variation in the fiber bending diameter was evaluated. The cladding intensity increased slightly when the core centre was launched by λ_{exD}. Spectral analysis showed a continuous increase in the donor peak λ_{emD} as the bending increased. For instance, Fig. 4b shows the output spectra of the fiber for different bending conditions and for a 406-nm input. The intensity was normalised with respect to the λ_{emD} peak to reveal changes in the Rhodamine 6G peak. In agreement with the principle depicted in Fig. 4a, the increase in the λ_{emA} peak was confirmed as the bending increased. Thus, the experimental results established that the fabricated structure could realise the proposed sensing principle [57]. In addition, the resolution of the fabricated sensor can be optimised by adjusting the waveguide parameters since a low-NA fiber exhibits enhanced sensitivity [57]. The sensor performance can also be enhanced by using better choices of materials with the excitation and emission wavelengths of the dyes matching the optical window of the host polymer [57].

Moreover, one possible interrogation technique for fused-POF-based sensors is to exploit the light intensity variations with respect to physical parameters, such as refractive index [59], acceleration [7], angle [60], temperature [61], torque [62], and strain [63]. Intensity variation-based fiber-optic sensors generally present the advantages of cost efficiency and simplicity of signal processing [54]. Recently, a dynamic mechanical analysis on the fused and non-fused POFs was performed [64], and the fused POFs were shown to be potentially higher in performance for strain sensing applications. Leal-Junior et al. [65] characterised the fused POFs for strain and transverse force sensing. The response of the fused POFs to these parameters were compared with those of the non-fused POFs. Afterwards, both fused and non-fused POFs were also characterised for temperature and moisture absorption, to evaluate the cross-sensitivity of the strain and transverse force sensors to these environmental parameters. The POF employed in the experiment had a perfluorinated graded-index core with 50 μm diameter made of doped polyperfluorobutenylvinyl ether, a cladding of the same material without doping with 25 μm thickness, and an overcladding (composed of polycarbonate) that resulted in an outer diameter of 750 μm.

Furthermore, the strain characterisation results revealed that the non-fused POF exhibited a strain sensitivity of $0.0060\%^{-1}$ which is 1.4 times higher than that of the fused POF ($0.0042\%^{-1}$). However, the fused POF demonstrated a higher linearity 0.999 than the non-fused POF (0.985). The root mean squared errors (RMSEs) between the reference strain applied and the one measured by the POF sensors for the fused and non-fused POFs with respect to the strain were 0.002% and 0.111%, respectively. Thus, the fused POFs possessed lower errors than the non-fused POFs. One possible reason for the high linearity of the fused POF is the linear relationship between stress and strain in this strain range. When the POF is under strain (or induced stress), its refractive index varies due to the stress-optic effect. The refractive index variation induces changes on the transmitted power owing to the variation of the critical angle and number of modes [66]. Thus, the linear deviations on the fiber stress may lead to linear variations of the POF power, which also accounts for the lower errors of the fused POF. The lower sensitivity of the fused POF can be attributed to its lower Young's modulus value which resulted in lower power attenuation than the non-fused POF [64, 65]. Moreover, the sensitivity of the fused POFs was higher in transverse force and temperature sensing, due to the higher sensitivity to the curvature that the transverse force creates on the POF and the more significant variations of the refractive index with temperature increase. Besides, the fused POFs exhibited lower moisture absorption than the non-fused POFs. The results obtained indicate a great potential of the fused POFs intensity-variation-based sensing applications of various physical parameters.

Multimodal interference-based strain sensors

Strain sensors based on the interference of multiple guided modes in multimode fibers (MMFs) have continued to attract considerable attention owing to their system simplicity, cost efficiency, and high sensitivity [67, 68]. Mizuno et al. [68] reported a strain sensor based on modal interference in a multimode fiber (MMF) comprising a perfluorinated graded-index POF (PFGI-POF). The MMF which serves as the sensing fiber was sandwiched between two single-mode fibers (SMFs)—a widely used configuration known as "single-mode- multimode-single-mode" (SMS) structure [67, 68]. The performance of the SMS-based strain sensor when strain is partially applied to fiber sections with different lengths was evaluated. The MMF was made of 1.0-m long PFGI-POF with a core diameter of 62.5 μm, a cladding diameter of 72.5 μm, and an overcladding diameter of 750 μm.

Strain was applied partially to the middle of the PFGI-POF using translation stages. The lengths of the strained sections were set to 0.1, 0.2, 0.4, 0.6, 0.8, and 0.93 m. The length of the whole POF excluding the connectors at both ends was 0.93 m. Irrespective of the lengths of the strained sections, the same amount of displacement of up to 500 μm was applied. Figures 5a and b illustrate the spectral dependence and dip wavelength dependence on displacement, respectively, when the length of the strained section was 0.93 m. As displacement was increased, the dip shifted to shorter wavelength with a dependence coefficient of − 48 pm/με. Figure 5c indicates the variation of the absolute value of the measured strain sensitivity with the length of the strained section.

The strain sensitivity was almost proportional to the strained length with a coefficient of 51.7 pm/με/m. Thus, the spectral dip shifts for the same amount of wavelength regardless of the strain magnitude or the strained length, provided the displacement of the POF is constant. Besides, the SMS-based strain sensors can be regarded as displacement sensors whether strain is applied to the whole length of the POF or only to part of the POF. The outcome of this investigation can form a relevant guideline for the application of SMS-based strain sensor to monitor conditions of civil structures.

Furthermore, most of the SMS-based sensors in the literature are two-end-access systems, in which both ends of the MMF are physically connected to SMFs. However, from a practical viewpoint, single-end-access configurations with an enhanced degree of freedom in embedding the sensors into structures are preferable. Kawa et al. [67] developed a single-end-access configuration of SMS-based strain and temperature sensing systems exploiting Fresnel reflection at the distal open end of the MMF (PFGI-POF).

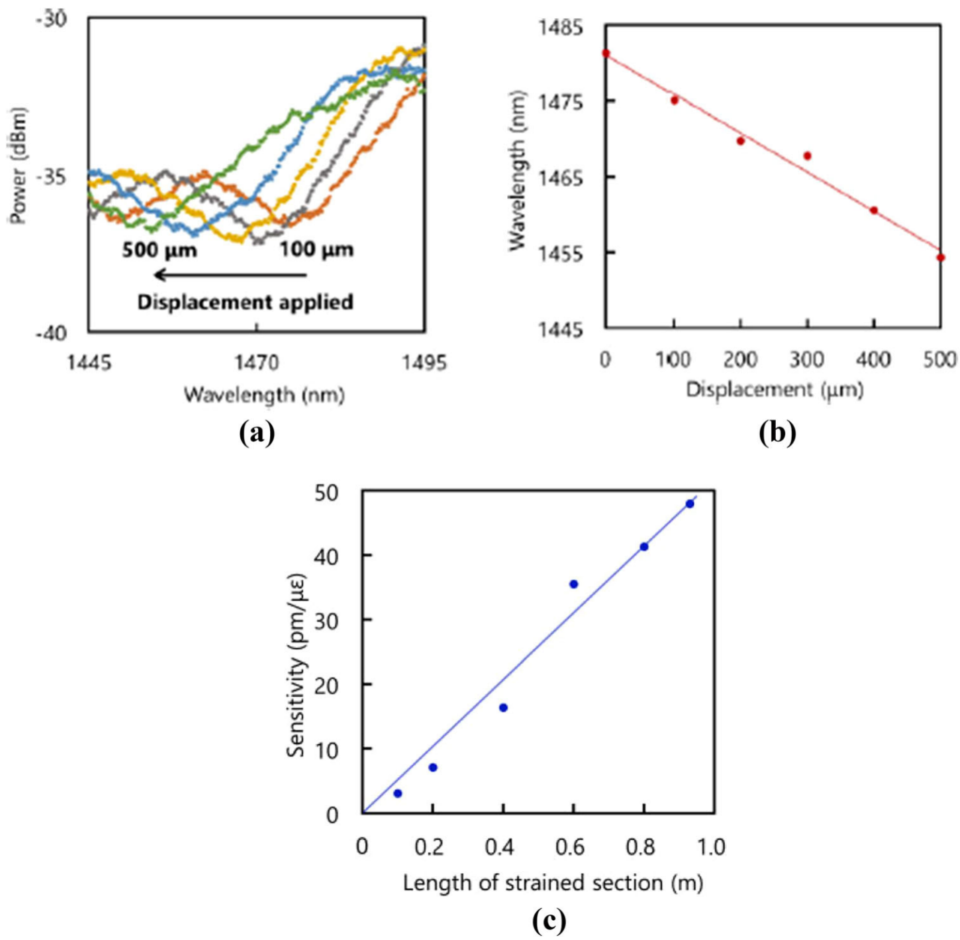

Fig. 5 **a** Applied displacement dependence of the spectral dip at 1470 nm when the length of the strained section was 0.93 m. **b** Corresponding dip wavelength plotted as a function of displacement. **c** Measured strain sensitivity (absolute value) plotted as a function of the length of the strained section. [68]

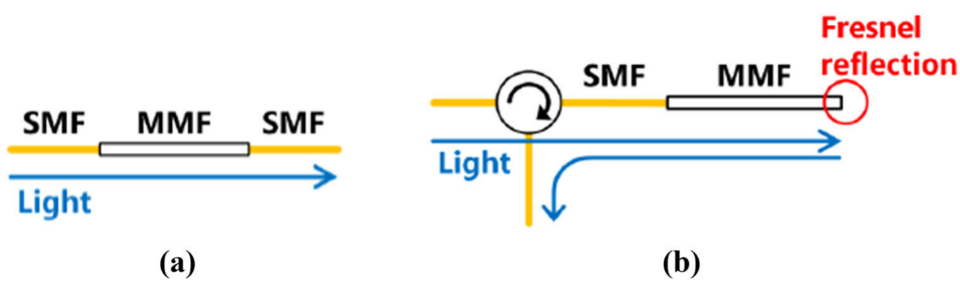

Fig. 6 Conceptual set-ups of **a** transmissive configuration and **b** reflectometric configuration. MMF, multimode fiber; SMF, single-mode fiber [67]

Figure 6a describes a conceptual set-up of the conventional two-end-access (or transmissive) configuration. When light is injected from an SMF to an MMF, a few lower modes are excited in the MMF owing to the spot-size difference between the fundamental (or 0th) modes in the SMF and the MMF. Assuming that the MMF and SMFs are axially aligned, the modes excited in the MMF are axially symmetric, and the optical power *P*out output from the SMS structure can be expressed as [69]

$$P_{out} = \left| a_0^2 + a_1^2 \exp i(\beta_0 - \beta_1)L + a_2^2 \exp i(\beta_0 - \beta_2)L + \ldots \right| \quad (5)$$

where a_i is the field amplitude of the *i*th mode at the first SMF-to-MMF interface, β_i is the propagation constant of the *i*th mode, and *L* is the MMF length. This equation indicates that the optical output power is influenced by physical changes (notably, the changes in the propagation constants and in the MMF length) caused by strain and temperature. Thus, by measuring the shift of spectral dips (or peaks), strain and temperature sensing can be performed. Figure 6b depicts a conceptual set-up of the single-end-access (or reflectometric) configuration. The light injected from an SMF into an MMF via an optical circulator is Fresnel-reflected at the distal open end of the MMF and then propagates back along the MMF and the SMF; the output spectrum is finally observed at the third port of the circulator. High strain and temperature sensitivities of – 122.2 pm/με and 10.1 nm/°C, respectively, were obtained. These values were comparable to those in the two-end-access configurations.

Brillouin-frequency-based strain sensors

Fiber-optic sensors exploiting Brillouin scattering have attracted considerable attention owing to their capability of entirely distributed measurement based on frequency information [70–73]. Their sensor heads are conventionally composed of glass optical fibers, which are easily broken when a strain of only ~3% is applied [74]. To extend the maximum measurable strain, polymer optical fibers (POFs) have been vigorously studied recently as alternatives to glass fibers because POFs are generally so flexible that they can withstand strains > 50% [75–79]. However, the maximal detectable strain using Brillouin scattering in POFs was a mere ~ 5%, because of a Brillouin-frequency-shift (BFS) hopping phenomenon accompanied by a slimming effect peculiar to polymer materials [80].

Furthermore, the BFS dependence on considerable strain in a slimmed POF was investigated by Mizuno et al. [80] to extend the strain dynamic range. The fiber under test (FUT) was made of a 0.58-m-long multimode perfluorinated graded-index (PFGI-) POF [81]. The POF had a three-layered structure consisting of core, cladding, and over-cladding (diameters: 50, 70, and 490 μm; refractive indices: ~ 1.35, ~ 1.34, and 1.59, respectively). Figure 7 describes the experimental set-up, which was based on self-heterodyne detection [82]. All the optical paths except the FUT were silica SMFs. The BFS was observed to be non-monotonically dependent on strain, in like manner with a non-slimmed POF, but without the BFS hopping phenomenon. With increasing strain, the BFS first decreased with a coefficient of –76.5 MHz/% (0–1.2% strain) and then increased with a coefficient of + 16.6 MHz/% (up to 30%). The BFS at 1.2–3.0% strain was almost independent of strain and cannot be directly used for strain sensing. This feature may potentially enable strain-insensitive temperature sensing by applying, for example, 2.0% strain to the slimmed POF beforehand. Besides, by applying 3.0% strain to a slimmed POF in advance, as large as > 25% strain can be measured simply by using the one-to-one correspondence of the BFS to the strain. This strain dynamic range was at least 5 times as wide as the conventional value using a non-slimmed POF.

Moreover, Wang et al. [83] proposed a wide-range strain sensor based on Brillouin frequency and linewidth in a 50 cm-long As_2Se_3-polymethyl methacrylate (As_2Se_3-PMMA) hybrid microfiber with a core diameter of 2.5 μm. The chalcogenide-PMMA (As_2Se_3-PMMA) hybrid optical fiber is fabricated by using chalcogenide (As_2Se_3) as the core and PMMA as the cladding. The hybrid structure provides sufficient mechanical robustness and flexibility, which allows the fabrication of tapers with As_2Se_3 core diameters at the sub-wavelength scale. The fabrication of As_2Se_3-PMMA taper was proposed due to its ultra-high nonlinearity $\gamma = 133\ (Wm)^{-1}$ [84]. Wang et al. [83] explored the possibility of using As_2Se_3-PMMA hybrid microfiber for wide-range strain sensing based on Brillouin optical time-domain analysis (BOTDA). No strain memory effect was observed over the15000 με range since Young's modulus for As_2Se_3 (17.8 GPa) [85] is larger than that of POF (3.5 GPa) [86]. Hence, the strain measurement is repeatable, even though the uncertainty is higher. Besides, the ultrahigh nonlinearity of As_2Se_3 enables low peak power of pump pulse for simulated Brillouin scattering (SBS) generation. For the first time, the authors demonstrated the Brillouin-frequency shift (BFS) and Brillouin linewidth dependence on strain over wide-range strain sensing in the As_2Se_3-PMMA hybrid microfiber.

The relationship between the BFS (υ_B) experienced by scattered light in the SBS process and longitudinal acoustic velocity (V_L) in the As_2Se_3-PMMA hybrid microfiber is given by [87]

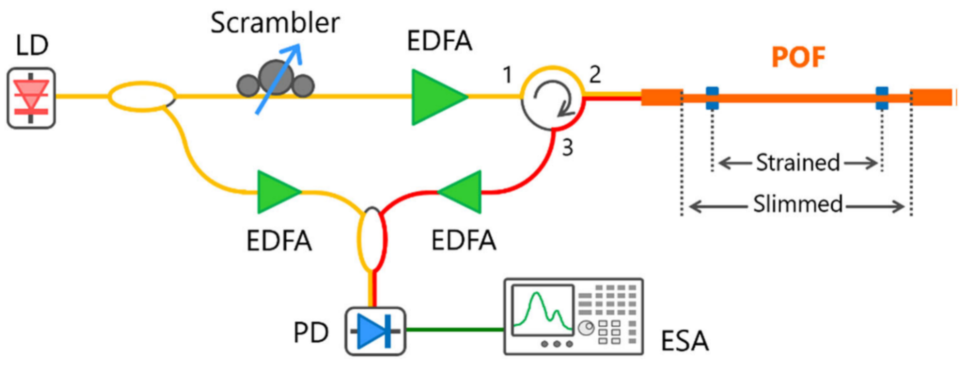

Fig. 7 Experimental set-up for investigating the strain dependence of the BFS in a slimmed POF. EDFA: erbium-doped fiber amplifier, ESA: electrical spectrum analyser, LD: laser diode, PD: photodetector [80]

$$\upsilon_B = \frac{2n_{eff}V_L}{\lambda_p} = \frac{2n_{eff}}{\lambda_p}\sqrt{\frac{1-\sigma}{(1-2\sigma)(1+\sigma)}\frac{E}{\rho}} \quad (6)$$

where λ_p is the pump wavelength, n_{eff} is the effective refractive index, σ is the Poisson's ratio, E is Young's modulus, and ρ is the density of the As_2Se_3 as the SBS occurs in the core of the hybrid fiber. Thus, the hybrid microfiber can be used for strain sensing based on BFS as the n_{eff} and V_L are dependent on the strain variation. The linear dependence between strain variation (Δε) and the change of BFS ($\Delta\upsilon_B$) is expressed as

$$\Delta\upsilon_B(\varepsilon) = \upsilon_B\left(\frac{1}{n_{eff}}\frac{\partial n_{eff}}{\partial\varepsilon} + \frac{1}{V_L}\frac{\partial V_L}{\partial\varepsilon}\right)\Delta\varepsilon \quad (7)$$

where $\frac{\partial n_{eff}}{\partial\varepsilon}$ is the photoelastic coefficient and $\frac{\partial V_L}{\partial\varepsilon}$ is the acousto-elastic coefficient.

The experimental results obtained demonstrated the linear strain dependence of the Brillouin-frequency shift and nonlinear dependence of the linewidth in a wide-range strain up to 15,000 με. When the strain was larger than 1500 με, the hybrid microfiber was deformed which was detected by measuring the distributed BFS and Brillouin linewidth. The strain errors obtained based on BFS measurement in the range of 0–1500 με and 1500–15,000 με were 42 με and 105 με, respectively. For strain dependence of Brillouin linewidth, the error was 65 με at 0–1500 με, and the maximum error of 353 με was recorded when the tensile strain was 15,000 με. The As_2Se_3-PMMA hybrid microfiber is a promising candidate for wide-range strain sensing owing to its ultrahigh nonlinear coefficient, small core size compared with POFs, and the low power requirement in pump pulse for SBS generation. The proposed strain sensor is suitable for monitoring civil infrastructures such as railway and bridge with steel structures that require large strain beyond that of SiO_2 limited to less than 1% [83].

Minakawa and Mizuno [74] examined the strain–temperature cross-sensitivity effect on the BFS in POFs. The strain and temperature dependencies of BFS are expressed by Eq. (6), which serves as the fundamental principle of Brillouin-based sensing. All the parameters in Eq. (6) except λ_p depend on strain and temperature [81, 88]. The BFS dependence on the strain at different temperatures was first measured, then followed by the BFS dependence on the temperature at different strains in the temperature range of 32–60 °C. The experimental results obtained showed that the strain coefficient of the BFS was dependent on the temperature. As indicated in Fig. 8, the temperature dependence of the BFS coefficient on the strain was linear with coefficients of 1.5 and – 0.3 MHz/(%·°C) in the strain ranges of 0–1.2% and 4.0–9.0%, respectively. Likewise, Fig. 9 shows that the temperature coefficient of the BFS exhibited a linear dependence on the strain with a coefficient of 1.5 and – 0.3 MHz/(%·°C), in the strain ranges of 0–1.2% and 4.0–9.0%, respectively. Therefore, to correctly detect the magnitudes of the strain and temperature in POF-based Brillouin sensing, temperature (and strain) compensation for the strain (and temperature) sensitivity of the BFS is required [74] [81]. However, it was confirmed experimentally that temperature sensing with no sensitivity to strain is potentially feasible using the BFS in POFs for strains > 13%.

Fabry–Perot (F-P) Cavity Strain Sensor

The large-range and high-sensitivity strain measurement in high-temperature ambiance is a great challenge in engineering applications [89]. Though the optical fiber made of silicon dioxide with a melting point of approximately 1700 °C has excellent high-temperature tolerance, its limited stretchability severely restricts the dynamic range of strain measurement. To overcome this limitation, Yi and Changyuan [89] developed a hybrid silica/polymer optical fiber Fabry–Perot (FP) cavity sensor, which can accommodate extraordinarily large strain at high temperatures. Figure 10a illustrates the structure of the hybrid silica/polymer F-P optical fiber sensor. The FP sensor consists of two silica up-taper fibers and a continuous polyimide (PI) tube with a length of L mm. The end faces of silica optical fiber can move freely as the PI tube stretches. The up-taper fibers used in the experiment were fabricated by a laser fusion tapering technique (Fujikura FSM-100). The CO_2 laser was focused on a standard commercial fiber (Corning SMF-28) with a core diameter of 8.2 μm and a cladding diameter of 125 μm, while the fiber was compressed with programmed moving platforms. Two up-taper fibers with flat end faces are inserted into the PI tube to form an F-P cavity sensor. The fibers were fixed with a little of high-temperature adhesive at two ends of the tube, separated by a distance L. Figure 10b describes the signal interrogation system and calibration system of the sensors.

Moreover, as depicted in Fig. 10b, the inverse relationship between the period of the reflected spectrum of F-P and the cavity length was verified theoretically and experimentally,). The experimental result strongly agreed with the theoretical result. The axial strain ε and the period of the reflected spectrum P also exhibit inversely proportional relationship, expressed as [89]

$$\varepsilon = \frac{\Delta l}{l_0} = \frac{\lambda_0^2}{2nl_0}\left(\frac{1}{P} - \frac{1}{P_0}\right) = \frac{\lambda_0^2}{2nl_0P} - 1 = \frac{P_0}{P} - 1 \quad (8)$$

where $P_0 = \frac{\lambda_0^2}{2nl_0P}$ is the initial period of the reflected spectrum corresponding to the initial cavity length l_0, Δl is

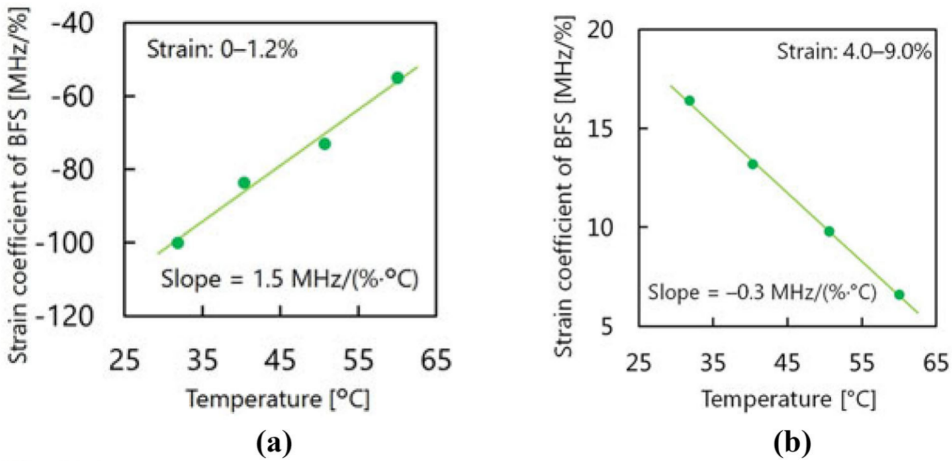

Fig. 8 Temperature dependence of the BFS coefficient on the strain **a** 0–1.2% **b** 4.0–9.0% [74]

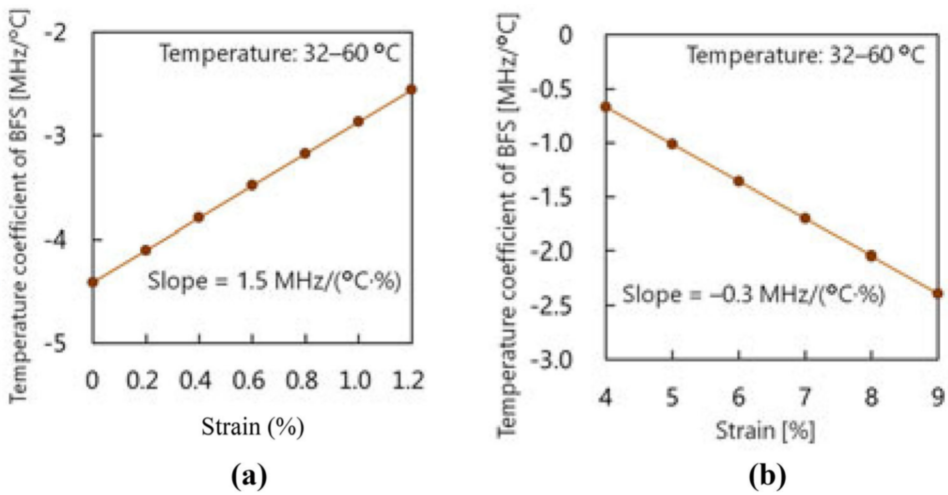

Fig. 9 Temperature coefficient of the BFS for strains of **a** 0–1.2% **b** 4.0–9.0% [74]

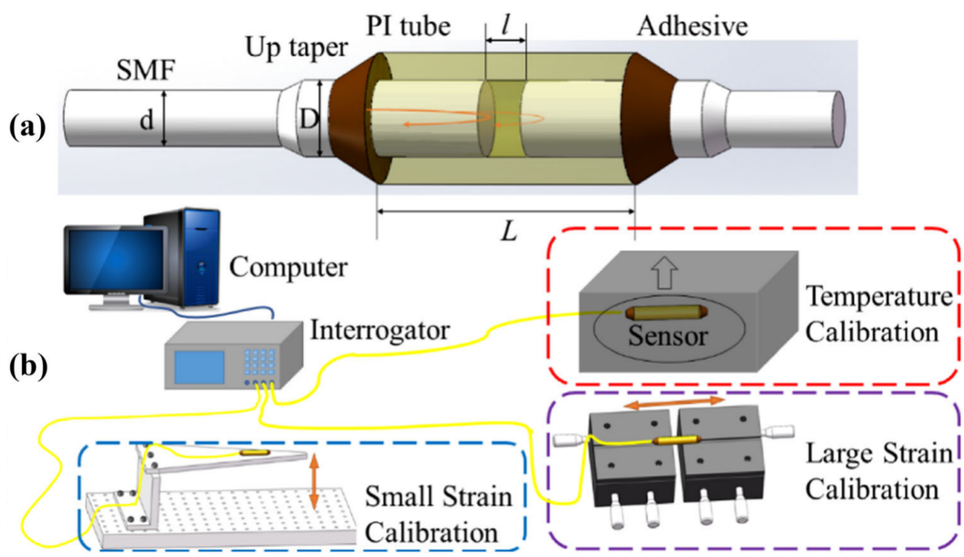

Fig. 10 **a** Schematic of a hybrid silica/polymer F-P optical fiber sensor structure and **b** the test system [89]

the cavity length change, l_0 is the initial cavity length, λ_0 is the optical wavelength in vacuum, and n is the refractive index in the air. According to Eq. (8), the axial strain in the PI tube can be determined using the cavity length change. Also, the strain sensitivity of the sensor can be expressed as

$$S = \frac{dP}{d\varepsilon} = -\frac{P_0}{(\varepsilon + 1)^2} \quad (9)$$

For large strain situation, Eq. (9) shows the strain sensitivity increases rapidly which corresponds to the cavity length longer than 200 µm. The simulation results show the sensor has a large dynamic range and high sensitivity [89].

According to the experimental results obtained, the proposed optical fiber sensor was able to withstand an ultimate tensile strain of 35%, which is 35 times larger than traditional fiber. A phase tracking method was used for the sensor to achieve high sensitivity of 28 pm/µε, which is 28 times larger than that of the traditional FBG sensors. Additionally, because of the excellent high-temperature endurance of PI and adhesive, the sensor can resist the high temperature of up to 220 °C. The large-strain, high-sensitivity, and high-temperature performances indicate that the proposed hybrid silica/polymer optical fiber F-P sensor has the potentials to monitor deformation in plastic products, structure health in composite materials such as carbon fiber reinforced polymer (CFRP) used for aircraft parts, and even strain in biomaterials.

Conclusion

The extremely high flexibility of POFs coupled with their unique capacity to tolerate strains of 50% or larger have earned them a centre stage in measuring stress and strain in a wide range of applications including structural health monitoring in civil construction and aerospace industries, biomedicine, and robotics. The recent developments in improving the sensitivity and dynamic range of POF strain sensors have been reviewed in this study under five main categories: fiber Bragg grating sensors, intensity-based sensors, multimodal interference-based sensors, Brillouin-frequency-based sensors, and Fabry–Perot cavity sensor. With a strain sensitivity of 0.701 ± 0.003 pm/µε combined with the ability to withstand high temperatures of up to 125 °C, the PC mPOFBGs have set the pace for the development of a reliable high-temperature-resistant polymer-based FBG with applications in automation technology and automotive. Tapered Chirped FBGs (CFBGs) are effective for strain sensing with a 3-dB bandwidth modulation remaining insensitive to humidity and temperature variations. The CFBG, inscribed in the endlessly single-mode BDK-doped PMMA mPOF, possessed a strain sensitivity of 0.90 ± 0.02 pm/µε, higher than that of a uniform POFBG in the same material and geometry ($\sim$0.71 pm/µε) due to the tapered etching of the fiber. The light coupling-based POF strain gauge offered a higher stability than the electronic type when applied to active orthosis for knee rehabilitation exercises. The strain dynamic range of the slimmed POF was boosted to measure as large as > 25% strain – five times as wide as the conventional value using a non-slimmed POF – obtained by using the one-to-one correspondence of the BFS to the strain. Additionally, the As_2Se_3-PMMA hybrid microfiber possesses huge potentials for wide-range strain sensing owing to its ultrahigh nonlinear coefficient, small core size compared with POFs, and the low power requirement in pump pulse for SBS generation. It is suitable for monitoring civil infrastructures such as railway and bridge with steel structures that require large strain beyond that of SOF. Moreover, it has been confirmed experimentally that temperature sensing with no sensitivity to strain is potentially feasible using the BFS in POFs for strains > 13%. The hybrid silica/polymer optical fiber F-P sensor is a top candidate for monitoring structural health in CFRP aircraft parts due to its high sensitivity, large dynamic range, and high temperature tolerance. The POF strain sensors are poised to continue their dominance over conventional strain sensors including SOF considering the steady improvement in their performance and dynamic range. Besides, the prime market for the POF strain sensor is projected to be the monitoring of civil engineering structures and earthworks.

References

1. D.J. Webb, Fiber Bragg grating sensors in polymer optical fibers. Meas. Sci. Technol. **26**(9), 2004 (2015)
2. F. Bischoff, Organic polymer biocompatibility and toxicology. Clin. Chem. **18**, 869 (1972)
3. M.C.J. Large, J. Moran, L. Ye, The role of viscoelastic properties in strain testing using microstructured polymer optical fiber (mPOF). Meas. Sci. Technol. **20**, 034014 (2009)
4. O.F. Dairo, A.O. Soge. "Polymer Optical Fibre in Communications and Environmental Monitoring". In Proceedings of Third National Conference of the Nigerian Union of Radio Science, Akure, Nigeria, (2010)
5. J. Zubia, J. Arrue, Plastic Optical Fibers: An introduction to their technological processes and applications. Opt. Fiber Technol. **7**, 101–140 (2001)
6. A.O. Soge, Polymer Optical Fibre Temperature Sensors - A Review. Asian J. Res. Rev. Phys. **3**(3), 19–37 (2020)
7. P.F.C. Antunes, H. Varum, P.S. Andre, Intensity-encoded polymer optical fiber accelerometer. IEEE Sens. J. **13**(5), 1716–1720 (2013)
8. D.W. Cullington, M.C.P. Hoar, Correcting for the effects of temperature on strain gauges —-use of computer–logger on Milford Haven Bridge project. Strain **11**(3), 99–103 (1975)
9. C.W. Silva, *Sensor Systems: Fundamentals and Applications*, 1st edn. (CRC Press, Boca Raton, 2016), pp. 455–467
10. A.T. Moraleda, C.V.J. Garciaa, Z. Zaballa, J. Arrue, A temperature sensor based on a polymer optical fiber macro-bend. Sensors (Basel) **13**(10), 13076–13089 (2013)
11. K. Peters, Polymer optical fiber sensors — a review. Smart Mater. Struct. **20**(1), 013002 (2011)

12. D. Webb, Polymer Fiber Bragg Grating Sensors and Their Applications, in *Optical Fiber Sensors: Advanced Techniques and Applications*. ed. by G. Rajan (CRC Press, Boca Raton, 2015), p. 19
13. M. Majumder, T.K. Gangopadhyay, A.K. Chakraborty et al., Fiber Bragg gratings in structural health monitoring—present status and applications. Sens. Actuators A: Phys. **147**(1), 150–164 (2008)
14. A. Panopoulou, T. Loutas, D. Roulias et al., Dynamic fiber Bragg gratings based health monitoring system of composite aerospace structures. Acta Astronaut. **69**(7–8), 445–457 (2011)
15. V. Mishra, N. Singh, U. Tiwari et al., Fiber grating sensors in medicine: current and emerging applications. Sens. Actuators A: Phys. **167**(2), 279–290 (2011)
16. A. Amjadi, K.U. Kyung, I. Park et al., Stretchable, skin-mountable, and wearable strain sensors and their potential applications: a review. Adv. Funct. Mater. **26**(11), 1678–1698 (2016)
17. R.M. Waxler, G. Cleek, Effect of temperature and pressure on refractive-index of some oxide glasses. J. Res. National Bureau Stand., Sect. A: Phys. Chem. **6**, 755–763 (1973)
18. L. Eldada, L.W. Shacklette, Advances in polymer integrated optics, Selected Topics in Quantum Electronics. IEEE J. Sel. Top. Quantum Electron. **6**(1), 54–68 (2000)
19. Z. Zhang, P. Zhao, P. Lin et al., Thermo-optic coefficients of polymers for optical waveguide applications. Polymer **47**, 4893–4896 (2006)
20. H.B. Liu, H.Y. Liu, G.D. Peng et al., Strain and temperature sensor using a combination of polymer and silica fiber Bragg gratings. Optics Commun. **219**, 139–142 (2003)
21. X.S. Cheng, W.W. Qiu, W.X. Wu et al., High-sensitivity temperature sensor based on Bragg grating in BDK-doped photosensitive polymer optical fiber. Chinese Opt. Lett. **9**(2), 020602 (2011)
22. T. Watanabe, N. Ooba, Y. Hida et al., Influence of humidity on refractive index of polymers for optical waveguide and its temperature dependence. Appl. Phys. Lett. **72**, 1533–1535 (1998)
23. W. Zhang, D.J. Webb, G.D. Peng, Investigation Into Time Response of Polymer Fiber Bragg Grating Based Humidity Sensors. J. Lightw. Technol. **30**, 1090–1096 (2012)
24. Pospori, A., Marques, C.A.F., Zubel, M.G., et al. (2016). "Annealing effects on strain and stress sensitivity of polymer optical fiber based sensors," *Proc. of SPIE,* vol. 9886, no. 1, https://doi.org/10.1117/12.2227473.
25. J. Capodagli, R. Lakes, Isothermal viscoelastic properties of PMMA and LDPE over 11 decades of frequency and time: A test of time-temperature superposition. Rheol. Acta **47**(7), 777–786 (2008)
26. A. Stefani, S. Andresen, W. Yuan et al., Dynamic Characterization of Polymer Optical Fibers. IEEE Sens. J. **12**, 3047–3053 (2012)
27. D. Sáez-Rodríguez, K. Nielsen, O. Bang, D.J. Webb, Time-dependent variation of fiber Bragg grating reflectivity in PMMA-based polymer optical fibers. Opt. Lett. **40**(7), 1476–1479 (2015)
28. I. Bundalo, K. Nielsen, G. Woyessa et al., Long-term strain response of polymer optical fiber FBG sensors. Opt. Mater. Express **7**(3), 967 (2017)
29. A. Abang, D.J. Webb, Effects of annealing, pre-tension and mounting on the hysteresis of polymer strain Sensors. Meas. Sci. Technol. **25**(1), 015102 (2014)
30. W. Yuan, A. Stefani, M. Bache et al., Improved thermal and strain performance of annealed polymer optical fiber Bragg gratings. Opt. Commun. **284**, 176–182 (2011)
31. G. Woyessa, K. Nielsen, A. Stefani, C. Markos, O. Bang, Temperature insensitive hysteresis free highly sensitive polymer optical fiber Bragg grating humidity sensor. Opt. Express **24**(2), 1206–1213 (2016)
32. K. Carroll, A. Argyros, K. Kalli et al., "Extending the working temperature range of Bragg gratings in microstructured polymer optical fiber by annealing". In Proceedings of the 16th International Conference on Plastic Optical Fibers (POF 2007), Turin, Italy, (2007)
33. S. Liehr, P. Lenke, M. Wendt et al., Polymer optical fiber sensors for distributed strain measurement and application in structural health monitoring. IEEE Sens. J. **9**(11), 1330–1338 (2009)
34. R. Ishikawa, H. Lee, A. Lacraz et al., Strain dependence of perfluorinated polymer optical fiber Bragg grating measured at different wavelengths. Jpn. J. Appl. Phys. **57**, 038002 (2018)
35. Y.J. Rao, In-fiber bragg grating sensors. Meas. Sci. Technol. **8**, 355 (1997)
36. M.G. Kuzyk, *Polymer Fiber Optics: Materials, Physics, and Applications, Boca Raton* (CRC Press, FL, 2006).
37. H. Ujihara, N. Hayashi, M. Tabaru et al., Measurement of large-strain dependence of optical propagation loss in perfluorinated polymer fibers for use in seismic diagnosis. IEICE Electron Express **11**, 20140707 (2014)
38. A. Fasano, G. Woyessa, P. Stajanca et al., Fabrication and characterization of polycarbonate microstructured polymer optical fibers for high-temperature-resistant fiber Bragg grating strain sensors. Opt. Mater. Express **6**, 649–659 (2016)
39. B. M. S. AG, "Optical properties of Makrolon and Apec for non-imaging optics," Bayer Material Science AG, 2014.
40. O. Ziemman, J. Krauser, P. E. Zamzow and W. Daum, POF Handbook. Optical Short Range Transmission Systems, Springer, 2008, p. Chap. 2.
41. M.C.J. Large, L. Poladian, G.W. Barton, M.A. van Eijkelenborg, *Microstructured Polymer Optical Fibers* (Springer, Berlin, 2008).
42. A. Stefani, W. Yuan, C. Markos et al., Narrow bandwidth 850-nm fiber bragg gratings in few-mode polymer optical fibers. IEEE Photonics Technol. Lett. **23**(10), 660–662 (2011)
43. I.P. Johnson, K. Kalli, D.J. Webb, 827nm Bragg grating sensor in multimode microstructured polymer optical fiber. Electron. Lett. **46**(17), 1217–1218 (2010)
44. W. Yuan, L. Khan, D.J. Webb et al., Humidity insensitive TOPAS polymer fiber Bragg grating sensor. Opt. Express **19**(20), 19731–19739 (2011)
45. C. Markos, A. Stefani, K. Nielsen et al., High-Tg TOPAS microstructured polymer optical fiber for fiber Bragg grating strain sensing at 110 degrees. Opt. Express **21**(4), 4758–4765 (2013)
46. K.E. Carroll, C. Zhang, D.J. Webb et al., Thermal response of Bragg gratings in PMMA microstructured optical fibers. Opt. Express **15**(14), 8844–8850 (2007)
47. W. Yuan, A. Stefani, M. Bache et al., Improved thermal and strain performance of annealed polymer optical fiber Bragg gratings. Opt. Commun. **284**(1), 176–182 (2011)
48. I.I. Bundalo, K. Nielsen, C. Markos et al., Bragg grating writing in PMMA microstructured polymer optical fibers in less than 7 minutes. Opt. Express **22**(5), 5270–5276 (2014)
49. D.X. Yang, J. Yu, X. Tao et al., Structural and mechanical properties of polymeric optical fiber. Mater. Sci. Eng. A **364**(1–2), 256–259 (2004)
50. R. Min, B. Ortega, C. Broadway et al., Microstructured PMMA POF chirped Bragg gratings for strain sensing. Optical Fiber Technol **45**, 330–335 (2018)
51. X. Hu, G. Woyessa, D. Kinet et al., BDK doped core microstructured PMMA optical fiber for effective Bragg grating photo inscription. Opt. Lett. **42**(11), 2209–2212 (2017)
52. A. Prospori, C.A.D. Marques, D. Sáez-Rodríguez et al., Thermal and chemical treatment of polymer optical fiber Bragg grating sensors for enhanced mechanical sensitivity. Opt. Fiber Technol. **36**, 68–74 (2017)

53. A.G. Leal-Junior, A. Frizera, C. Marques et al., Polymer optical fiber strain gauge for human-robot interaction forces assessment on an active knee orthosis. Opt. Fiber Technol. **41**, 205–211 (2018)
54. L. Bilro, N. Alberto, J.L. Pinto et al., Optical sensors based on plastic fibers. Sensors (Switzerland) **12**(9), 12184–12207 (2012)
55. T. Becker, O. Ziemann, R. Engelbrecht et al., Optical strain measurement with step-index polymer optical fiber based on the phase measurement of an intensity-modulated signal. Sensors **18**, 2319 (2018)
56. Liehr, S., Lenke, P., Krebber, K. et al. (2008). "Distributed strain measurement with polymer optical fibers integrated into multi-functional geotextiles. Proceedings of the Conference Optical Sensors," in *Proceedings of the Conference Optical Sensors*, Strasbourg, France.
57. S. Kamimura, R. Furukawa, Strain sensing based on radiative emission-absorption mechanism using dye-doped polymer optical fiber. Appl. Phys. Lett. **111**, 063301 (2017)
58. Furukawa, R., Mizorogi, D., Tsukada, K., et al. (2014). "Stress-induced light leakage of rhodamine 6G doped polymer optical fiber. in *Proceedings of the 23rd International Conference on Plastic Optical Fibers* (POF 2014)," Kanagawa, Japan.
59. A.R. Prado, A.G. Leal-Junior, C.C. Marques et al., Polymethyl methacrylate (PMMA) recycling for the production of optical fiber sensor systems. Opt. Express **25**(24), 30051–30060 (2017)
60. A.G. Leal-Junior, A.A. Frizera, M.J. Pontes, Dynamic Compensation Technique for POF Curvature Sensors. J. Lightwave Technol. **36**(4), 1112–1117 (2018)
61. A. Leal-Junior, A. Frizera-Neto, C. Marques et al., A polymer optical fiber temperature sensor based on material features. Sensors (Basel) **18**(2), 301 (2018)
62. A.G. Leal-Junior, A. Frizera, C. Marques et al., Polymer optical fiber for angle and torque measurements of a series elastic actuator's spring. J. Lightw. Technol. **36**(9), 1698–1705 (2018)
63. D.Z. Stupar, J.S. Bajić, B.M. Dakić et al., The possibility of using a plastic optical fiber as a sensing element in civil structural health monitoring. Phys. Scr. T. **157**, 014031 (2013)
64. A. Leal-Junior, A. Frizera, M.J. Pontes et al., Dynamic mechanical analysis on fused polymer optical fibers: towards sensor applications. Opt. Lett. **43**(8), 1754–1757 (2018)
65. A. Leal-Junior, A. Frizera, H. Lee et al., Strain, temperature, moisture, and transverse force sensing using fused polymer optical fibers. Opt. Express **26**(10), 12939–12947 (2018)
66. A.G. Leal-Junior, A. Frizera, M.J. Pontes, Analytical model for a polymer optical fiber under dynamic bending. Opt. Laser Technol. **93**, 92–98 (2017)
67. Kawa, T., Numata, G., Lee, H., et al. (2017). "Single-end-access strain and temperature sensing based on multimodal interference in polymer optical fibers," *IEICE Electronics Express, 14*(3), doi: https://doi.org/10.1587/elex.14.20161239.
68. Y. Mizuno, S. Hagiwara, T. Kawa et al., Displacement sensing based on modal interference in polymer optical fibers with partially applied strain. Jpn. J. Appl. Phys. **57**, 058002 (2018)
69. A. Kumar, R.K. Varshney, P. Sharma, Transmission characteristics of SMS fiber optic sensor structures. Opt. Commun. **219**(1–6), 215–219 (2003)
70. T. Horiguchi, T. Kurashima, M. Tateda et al., Tensile strain dependence of Brillouin frequency shift in silica optical fibers. IEEE Photon. Technol. Lett. **1**(5), 107–108 (2002)
71. Y. Mizuno, W. Zou, Z. He et al., Proposal of Brillouin optical correlation-domain reflectometry (BOCDR). Opt. Express **16**, 12148–12153 (2008)
72. Y. Dong, B. Dexin, T. Jiang et al., BOTDA for dynamic strain measurement based on differential double-pulse and second-order sideband of modulation. IEEE Photon. **5**(3), 2600407 (2013)
73. Y. Mizuno, N. Hayashi, H. Fukuda et al., Ultrahigh-speed distributed Brillouin reflectometry. Light Sci. Appl. **5**, e16184 (2016)
74. K. Minakawa, K. Mizuno, Cross effect of strain and temperature on brillouin frequency shift in polymer optical fibers. J. Lightw. Technol. **35**(12), 2481 (2017)
75. A. Minardo, R. Bernini, L. Zeni, Distributed temperature sensing in polymer optical fiber by BOFDA. IEEE Photon. Technol. Lett. **26**(4), 387–390 (2014)
76. Y. Dong, P. Xu, H. Zhang et al., Characterization of evolution of mode coupling in a graded-index polymer optical fiber by using Brillouin optical time-domain analysis. Opt. Express **22**, 26510–26516 (2014)
77. N. Hayashi, Y. Mizuno, K. Nakamura, Distributed Brillouin sensing with centimeter-order spatial resolution in polymer optical fibers. J. Lightw. Technol. **32**(21), 3999–4003 (2014)
78. N. Hayashi, K. Minakawa, Y. Mizuno et al., Brillouin frequency shift hopping in polymer optical fiber. Appl. Phys. Lett. **105**, 091113 (2014)
79. H. Ujihara, N. Hayashi, M. Tabaru et al., Measurement of large-strain dependence of optical propagation loss in perfluorinated polymer fibers for use in seismic diagnosis. IEICE Electron. Express **11**, 20140707 (2014)
80. Y. Mizuno, N. Matsutani, N. Hayashi et al., Brillouin characterization of slimmed polymer optical fibers for strain sensing with extremely wide dynamic range. Opt. Express **26**(21), 28030–28037 (2018)
81. Y. Koike, M. Asai, The future of plastic optical fiber. NPG Asia Mater. **1**(1), 22–28 (2009)
82. Y. Mizuno, K. Nakamura, Experimental study of Brillouin scattering in perfluorinated polymer optical fiber at telecommunication wavelength. Appl. Phys. Lett. **97**(2), 021103 (2010)
83. H. Wang, S. Gao, C. Baker et al., Wide-range strain sensor based on Brillouin frequency and linewidth in an As2Se3-PMMA hybrid microfiber. Opt. Express **28**(15), 22933–22945 (2020)
84. C. Baker, M. Rochette, Highly non-linear hybrid asse-pmma microtapers. Opt. Express. **18**(12), 12391–12398 (2010)
85. N. Soga, M. Kunugi, R. Ota, Elastic properties of Se and As2Se3 glasses under pressure and temperature. J. Phys. Chem. Solids **34**(12), 2143–2148 (1973)
86. C. Ishiyama, Y. Higo, Effects of humidity on young's modulus in poly (methyl methacrylate). J. Polym. Sci., Part B: Polym. Phys. **40**(5), 460–465 (2002)
87. C. Zhang, W. Li, X. Bao et al., Tensile strain dependence of the brillouin gain spectrum in carbon/polyimide coated fibers. Opt. Lett. **32**(17), 2565–2567 (2007)
88. Y. Mizuno, N. Hayashi, K. Nakamura, Fresnel-assisted self-heterodyne detection for Brillouin gain spectrum characterisation in polymer optical fibers. Electron. Lett. **50**, 1153–1155 (2014)
89. L. Yi, Y. Changyuan, Highly stretchable hybrid silica/polymer optical fiber sensors for large-strain and high temperature application. Opt. Express **27**(15), 20107–20116 (2019)